THE JOURNAL OF BIOLOGICAL CHEMISTRY VOL. 290, NO. 32, pp. 19629–19640, August 7, 2015

Structural Basis for Antibody Recognition of Lipid A

INSIGHTS TO POLYSPECIFICITY TOWARD SINGLE-STRANDED DNA[*]

Received for publication, April 12, 2015, and in revised form, May 29, 2015 Published, JBC Papers in Press, June 17, 2015, DOI 10.1074/jbc.M115.657874

Omid Haji-Ghassemi[‡], **Sven Müller-Loennies**[§1], **Teresa Rodriguez**[‡], **Lore Brade**[§], **Paul Kosma**[¶], **Helmut Brade**[§], **and Stephen V. Evans**[‡2]

From the [‡]*Department of Biochemistry and Microbiology, University of Victoria, Victoria, British Columbia V8P 3P6, Canada, the* [§]*Research Center Borstel, Leibniz-Center for Medicine and Biosciences, Parkallee 22, Borstel D-23845, Germany, and the* [¶]*Department of Chemistry,* [¶]*University of Natural Resources and Life Sciences, 1190 Vienna, Austria*

Background: Lipid A-specific antibodies are not effective in sepsis treatment; infection by Gram-negative bacteria can induce autoimmune disease.
Results: Antibody-combining sites orient lipid A to bury the LPS attachment point and can cross-react with ssDNA through terminal nucleotides.
Conclusion: Anti-lipid A antibodies cannot bind full-length LPS; phosphates play a crucial role in polyspecificity.
Significance: Antibody recognition of lipid A illuminates the genesis of autoimmunity.

Septic shock is a leading cause of death, and it results from an inflammatory cascade triggered by the presence of microbial products in the blood. Certain LPS from Gram-negative bacteria are very potent inducers and are responsible for a high percentage of septic shock cases. Despite decades of research, mAbs specific for lipid A (the endotoxic principle of LPS) have not been successfully developed into a clinical treatment for sepsis. To understand the molecular basis for the observed inability to translate *in vitro* specificity for lipid A into clinical potential, the structures of antigen-binding fragments of mAbs S1–15 and A6 have been determined both in complex with lipid A carbohydrate backbone and in the unliganded form. The two antibodies have separate germ line origins that generate two markedly different combining-site pockets that are complementary both in shape and charge to the antigen. mAb A6 binds lipid A through both variable light and heavy chain residues, whereas S1–15 utilizes exclusively the variable heavy chain. Both antibodies bind lipid A such that the GlcN-O6 attachment point for the core oligosaccharide is buried in the combining site, which explains the lack of LPS recognition. Longstanding reports of polyspecificity of anti-lipid A antibodies toward single-stranded DNA combined with observed homology of S1–15 and A6 and the reports of several single-stranded DNA-specific mAbs prompted the determination of the structure of S1–15 in complex with single-stranded DNA fragments, which may provide clues about the genesis of autoimmune diseases such as systemic lupus erythematosus, thyroiditis, and rheumatic autoimmune diseases.

Bacterial Gram-positive and Gram-negative infections are a leading cause of septic shock, with over 750,000 cases annually in the United States and with a mortality rate between 28 and 50% (1–3). It is the third most common cause of death in Germany where it claims 60,000 lives a year (2). The inflammatory cascade at the onset of septic shock can be caused by the presence of bacterial lipopolysaccharide (LPS), which is shed from the outer membrane of Gram-negative bacteria (4).

The inflammatory cascade is initiated by the formation of a signaling complex of the lipid A moiety of LPS with Toll-like receptor 4 (TLR4) and co-receptor myeloid differentiation factor 2 (MD-2) (5–8). One heavily investigated therapeutic route has been focused on the potential of monoclonal antibodies (mAbs) to sequester LPS (9–11) to prevent formation of the LPS·MD-2·TLR4 signaling complex. Although antibodies specific for the lipid A, core, and *O*-polysaccharide components of LPS have been reported (10–19), the diversity of structures together with the rapid onset of septic shock have hindered the introduction of *O*-polysaccharide-specific antibodies into clinical use (4, 11, 20–22). In contrast to *O*-polysaccharide, there is strong structural conservation among the inner cores of relevant serovars (23); however, generation of broadly cross-reactive antibodies has proved challenging. To date, only mAb WN1 222-5 has been reported to be successful in neutralizing a wide range of Gram-negative bacteria, including *Escherichia*, *Salmonella*, *Shigella*, and *Citrobacte*r (9, 10, 24).

Although lipid A structure is relatively conserved among pathogenic species, none of the numerous reported antibodies claimed to be specific for lipid A have led to successful clinical implementation (13–15, 25). Specific binding to lipid A was observed upon acid treatment of bacterial LPS, thereby liberating the lipid A fragment acting then as neoantigen, when embedded into erythrocytes or liposomes (25, 26). Of particular significance were mAbs A6 (IgG2b) isolated from mice immunized with heat-killed *Escherichia coli* J-5 cells (27) and S1–15, also referred to as S1 (25). Binding studies showed a preference of mAb A6 for the bisphosphorylated (*i.e.* native) lipid A, with weak binding to the monophosphorylated lipid A

[*] This work was supported by the Natural Sciences and Engineering Research Council of Canada (to S. V. E.) and by Austrian Science Fund (Fonds zur Förderung der Wissenschaftlichen Forschung) Grant P22909 (to P. K.). The authors declare that they have no conflicts of interest with the contents of this article.

The atomic coordinates and structure factors (codes 4ODS, 4ODT, 4ODU, 4ODV, 4ODW, 4Z8F, and 4Z95) have been deposited in the Protein Data Bank (http://wwpdb.org/).

[1] To whom correspondence may be addressed. E-mail: sml@fz-borstel.de.
[2] To whom correspondence may be addressed. E-mail: svevans@uvic.ca.

(25), although S1–15 displays high avidity for both the mono- and bisphosphorylated lipid A (25, 28). Neither antibody was observed to recognize intact LPS.

Our earlier work showed that such antibodies bind as well to the bisphosphorylated glucosamine (GlcN) disaccharide backbone (BBP)[3] without the acyl chains (28), indicating that S1–15 and A6 recognize the carbohydrate backbone exclusively. Significantly, binding studies of the C6′ methyl-capped disaccharide showed that neither antibody bound lipid A lacking a free primary hydroxyl at C6 on the β-GlcN, which serves as the attachment point for inner core residues of the LPS (29).

Interestingly, a number of anti-lipid A antibodies have been reported to display significant polyspecificity to a range of antigens, including cardiolipin (30, 31), I antigen on B-lymphocytes (30), double-stranded DNA (dsDNA) (13), and single-stranded DNA (ssDNA) (14, 30), with reports of mice immunized with bacterial LPS resulting in mAbs cross-reactive to DNA (32, 33). Antibodies against ssDNA are noteworthy, as their induction has been implicated in autoimmune diseases such as lupus (34–37), thyroid disease (38), and rheumatic disorders (31, 39). Furthermore, studies have implicated a specific variable heavy chain family gene V(H)4–21 in dual recognition of lipid A and ssDNA, demonstrating a possible link between infection with Gram-negative bacteria and development of systemic lupus erythematosus and arthritis (31, 34).

To date there are no reports of crystal structures of any anti-lipid A mAb either unliganded or in complex. We now report binding data and crystal structures of unliganded and liganded antigen-binding fragments (Fabs) for two anti-lipid A mAbs, S1–15 and A6, to elucidate the reason these antibodies do not bind intact LPS. Furthermore, we present a structure of S1–15 in complex with ssDNA fragments that supports the polyspecific potential of anti-lipid A antibodies toward ssDNA.

Experimental Procedures

ELISA—ELISA against the immobilized neoglycoconjugates was performed as described earlier (29). For the binding assay, BBP and B4P were conjugated in a 5 M excess to BSA, which had been activated by divinylsulfone, were then immobilized at concentrations of 2.5, 5.0, 10, and 20 pmol of ligand per well, and reacted with mAbs A6 and S1–15, which were titrated 1:1 over 12 steps starting from 2 μg/ml concentration.

Germ Line Gene Usage Analysis—The nucleotide sequences of the variable regions were analyzed with the IMGT/V-quest and junctional analysis web applications (40, 41) to determine the murine germ line gene segments from which the lipid A-specific antibodies were derived.

Fab Preparation and Crystallization—Generation of mAbs S1–15 (IgG_{2b}) (25) and A6 (IgG_{2b}) (27) was described earlier. For large scale preparation, mAb S1–15 was isolated from ascites by affinity chromatography on BBP conjugated to AH-Sepharose (80 mg of ligand/2.5 ml of packed beads) followed by elution with 0.1 M glycine-HCl, pH 3.2 (29). Fractions were adjusted to pH 4 by addition of 1 M $NaHCO_3$. Antibody A6 was isolated and purified in the same manner as S1–15.

Fab fragments of each antibody were prepared by digestion of the intact immunoglobulin with papain (Sigma). IgG was dialyzed into 25 mM HEPES (Sigma), pH 7.5, diluted to a concentration of 1.0–0.8 mg/ml, 2 mM EDTA (Sigma), and 5–6 mM DTT (Sigma). The digestion reaction was carried out at room temperature using a papain/IgG ratio of 1:200 molar eq for 2–3 h. The reaction was quenched by the addition of 10 mM iodoacetamide (Sigma) and dialyzed overnight into 25 mM HEPES buffer, pH 7.4. Fab fragment was purified by cation-exchange chromatography on a Shodex CM-825 column (Phenomenex, Torrance, CA) using a linear gradient of 0.0 to 0.5 M NaCl in 20 mM HEPES, pH 7.4. Purified Fab was concentrated to 10–12 mg/ml stock and stored at 4.0 °C.

The Fabs of A6 and S1–15 mAbs were mixed with 3 mM lipid A backbone bisphosphate: βGlcN4*P*(1→6)αGlcN1*P*, designated BBP (28), for liganded crystallization screening. Several crystals ($0.25 \times 0.35 \times 0.30$ mm^3) were obtained for S1–15 in the presence of BBP after 2 months in a 16 °C room from hanging drop setup in PEG II suite crystal screen (Qiagen, Toronto, Canada), under condition 13 (0.1 M sodium chloride, 0.1 M bicine, pH 9.0, and 30% (w/v) PEG 550 methyl ether) using a 1:1 reservoir-to-protein ratio. Approximately cubic crystals ($0.1 \times 0.15 \times 0.15$ mm^3) of A6 were grown initially at a hanging drop setup in a 16 °C room in the presence of BBP using Index crystal screen (Hampton Research, Aliso Viejo, CA) under condition 44 (0.1 M HEPES, pH 7.5, and 25% (w/v) PEG 3350) in 1:1 reservoir-to-protein ratio. Larger crystals ($0.4 \times 0.4 \times 0.2$ mm^3) were obtained using a 1:1.5 reservoir-to-protein ratio.

Fresh papain digests of intact S1–15 and A6 were used by applying the protocol as above, for crystallization screening of unliganded Fabs and S1–15 Fab in the presence of oligonucleotides. Conditions were set using an Art Robbins Gryphon Xtallization Robot (San Jose, CA), with each 96-well sitting drop plate incubated in a 16 °C room. S1–15 unliganded crystals ($0.4 \times 0.3 \times 0.25$ mm^3) were grown under condition 21 (25% (w/v) PEG 2000 MME) of the PEG II suite screen. Initial crystals of variable sizes for unliganded A6 Fab were grown under condition 16 (0.1 M Tris-HCl, pH 8.5, and 30% (w/v) PEG 1000) of PEG II suite crystal screen, and subsequently optimized (for diffraction quality) using 35% (w/v) PEG 1000. S1–15 Fab (12 mg/ml) was mixed with the deoxythymidine oligonucleotides of sequence 5′*P*-TTTTT-3′*P* (both ends phosphorylated) referred to as *p*5(dT)*p* and 5′-TTTTT-3′*P* (lacking the 5′-phosphate) referred to as 5(dT)*p*, in a 1:2 molar ratio. Crystals in presence of *p*5(dT)*p* oligonucleotides were initially obtained after a few days using the sitting drop method under condition 55 (0.075 M $MgCl_2$, 0.1 M HEPES, pH 7.5, 28% (v/v) PEG 550 MME) of the index screen (Hampton Research). Larger crystals ($0.35 \times 0.3 \times 0.3$ mm^3) were obtained via the hanging drop method and using 1:2–1:3 reservoir-to-protein ratios. A large crystal ($0.7 \times 0.4 \times 0.4$ mm^3) was obtained in presence of 5(dT)*p* antigen, after a few days under condition 22 (0.1 M Tris-HCl, pH 8.5, 25% (v/v) PEG 550 MME) of the PEG suite crystal screen using sitting drop method.

[3] The abbreviations used are: BBP, bisphosphorylated lipid A backbone; CDR, complementarity determining region; Fab, fragment antigen binding; Fv, fragment variable; GlcN, D-glucosamine; V_H, variable heavy; V_L, variable light; B4P, 4′-monophosphorylated lipid A backbone; DVS, divinyl sulfone; ssDNA, single-stranded DNA; bicine, *N*,*N*-bis(2-hydroxyethyl)glycine; r.m.s.d., root mean square deviation.

Data Collection, Molecular Replacement, and Structure Refinement—Crystallization conditions for S1–15 liganded and unliganded, as well as A6 unliganded structures already contained levels of cryoprotectant suitable to form a glass upon freezing. Liganded A6 crystals were carefully dehydrated in a 16 °C room until the concentration of cryoprotectant (PEG 3350) reached appropriate levels. All crystals were flash-frozen to −160 °C using an Oxford Cryostream 700 crystal cooler (Oxford Cryosystems, Oxford, UK). The x-ray diffraction data sets were collected at the Canadian Macromolecular Crystallography Facility on beamline 08ID-1 of the Canadian Light Source (Saskatoon, Saskatchewan, Canada) at 0.979 Å wavelength, with a Marmosaic CCD300 detector, and processed using HKL2000 (HKL Research Inc., Charlottesville, VA).

The S1–15 structure in complex with lipid A was solved by molecular replacement using Phaser (42) with the constant domain and Fv fragments of unliganded Fab S55–3 (Protein Data Bank code 4ODS) as search models. The liganded structure of S1–15 was used subsequently as a search model for the unliganded S1–15 dataset and the ssDNA liganded datasets. The A6 liganded structure was also solved using the Fv and constant domains of the S1–15 liganded structure as search models. The liganded Fv and constant domains of A6 Fab were used as search models for the unliganded A6 structure.

Manual fitting of σ-A-weighted $F_o - F_c$ and $2F_o - F_c$ electron density maps was carried out with Coot (43). Restrained refinement and translation, libration, and screw (TLS) refinement was carried out using REFMAC5 (44, 45). All stereo figures and r.m.s.d. calculations presented in this paper were made using SetoRibbon (available upon request from author S. V. E.). Electrostatic surface potential figures were made using Chimera molecular visualization software (46). Marvin Sketch Version 5.7.0 from ChemAxon was used for drawing chemical structures.

Results

Characterization of Lipid A-specific Antibodies through ELISA—The quantitative conjugate ELISA for mAbs S1–15 and A6 to BBP and B4P at concentrations of 2.5, 5, 10, and 20 pmol/well are shown in Fig. 1. Both antibodies bound to the immobilized BBP conjugate and much weaker to the B4P conjugate. Against BBP, the affinity of S1–15 was ~4-fold weaker than A6. However, S1–15 showed stronger binding to the B4P-conjugate confirming the weaker dependence on the recognition of the phosphate at the anomeric position (25). Binding data against synthetic lipid A and derivatives thereof have been reported earlier (15, 25, 29).

X-ray Diffraction Data Collection and Refinement—Data collection and refinement statistics for liganded and unliganded structures of the Fabs from lipid A-specific mAbs S1–15 (IgG_{2b}) and A6 (IgG_{2b}) are given in Table 1. Deacylated and purified lipid A (BBP) was used during crystallization trials (Fig. 1*C*).

A6—Data were collected to 2.15 Å resolution from a crystal grown in the presence of BBP, which were consistent with orthorhombic space group $P2_12_12_1$ with an R_{sym} of 0.085 and containing one molecule per asymmetric unit. Superb electron density was observed for the antigen (Fig. 2*A*) and for the remainder of the protein, with the exception of the solvent-exposed residues 128–136 and 157–161 on the H chain constant domain, which is often observed to be disordered in IgG_{2b} Fab structures (47–50). Data were collected on crystals of the unliganded Fab of A6 to 2.75 Å resolution with R_{sym} of 0.041 in triclinic space group *P*1. The structure was solved with two molecules in the asymmetric unit, and it exhibited relatively higher thermal motion that manifested as poor electron density in solvent-exposed regions, particularly residues 127–134 and 157–161 on the constant domain of the H chain, some of which were excluded from the final model.

S1–15—Data of crystals of S1–15 grown in the presence of BBP collected to 1.95 Å resolution fit a tetragonal unit cell in Laue group 422 with an R_{sym} of 0.088 and with systematic absences corresponding to space groups $P4_12_12$ and $P4_32_12$. The structure was solved in space group $P4_32_12$ by molecular replacement with one molecule in the asymmetric unit. Excellent electron density was observed for the antigen (Fig. 2*B*) and for the remainder of the protein with the exception of residues in the corresponding region as A6 structures.

Data for two additional liganded S1–15 Fab structures were collected as follows: one in complex with 5-stranded deoxythymidine (dT) oligonucleotide with both ends phosphorylated or *p*5(dT)*p* and a 5-oligothymidine nucleotide with no 5′-terminal phosphate called 5(dT)*p*. The data were collected to 1.75 and 1.79 Å resolution with R_{sym} of 0.059 and 0.053, respectively (Table 1). Both data sets were solved in the same space group and near-identical unit cells as the structure of S1–15 in complex with the lipid A analogue. The ssDNA ligand with both terminal phosphates showed density for two separate oligonucleotide fragments, one at each phosphate-binding site of lipid A. A dinucleotide with the 3′-terminal phosphate occupies the 1*P* lipid A recognition pocket, and on the 4*P* lipid A pocket, a trinucleotide could be confidently modeled, although the terminal 5′-thymine base was largely disordered. The two oligonucleotide fragments stabilized one another through stacking interactions via symmetry-related Fab molecules, showing electron density corresponding to a total of five oligonucleotides (Fig. 2*C*). In the second data set with 5(dT)*p* as ligand, density could only be observed for the 3′-phosphate group (Fig. 2*D*) as the rest of the oligonucleotide could not be modeled due to dynamic disorder.

Data were collected on the unliganded of S1–15 Fab to 2.29 Å resolution with R_{sym} of 0.063 and were solved in the monoclinic space group $P2_1$ containing two molecules in the asymmetric unit. As with the liganded structures, residues 128–132 on the H chain were disordered with some residues excluded from the final model.

Germ Line Gene Usage and Sequence Comparison—The primary sequence comparisons for the variable loops of mAbs S1–15 and A6 are given in Table 2. IMGT germ line database analysis revealed that the nucleotide sequences of mAbs S1–15 and A6 arise from closely related V- and J-genes for the V_L chain. The A6 V_L chain was found to share 261/279 and 36/39 nucleotide identity with *V*-gene IGKV10–96*01 and J-gene IGKJ1*02, respectively (the * denotes the allele group). The S1–15 V_H chain was found to share 292/294 nucleotide identity with the *V*-gene IGHV10–1*02, resulting in a single mutation

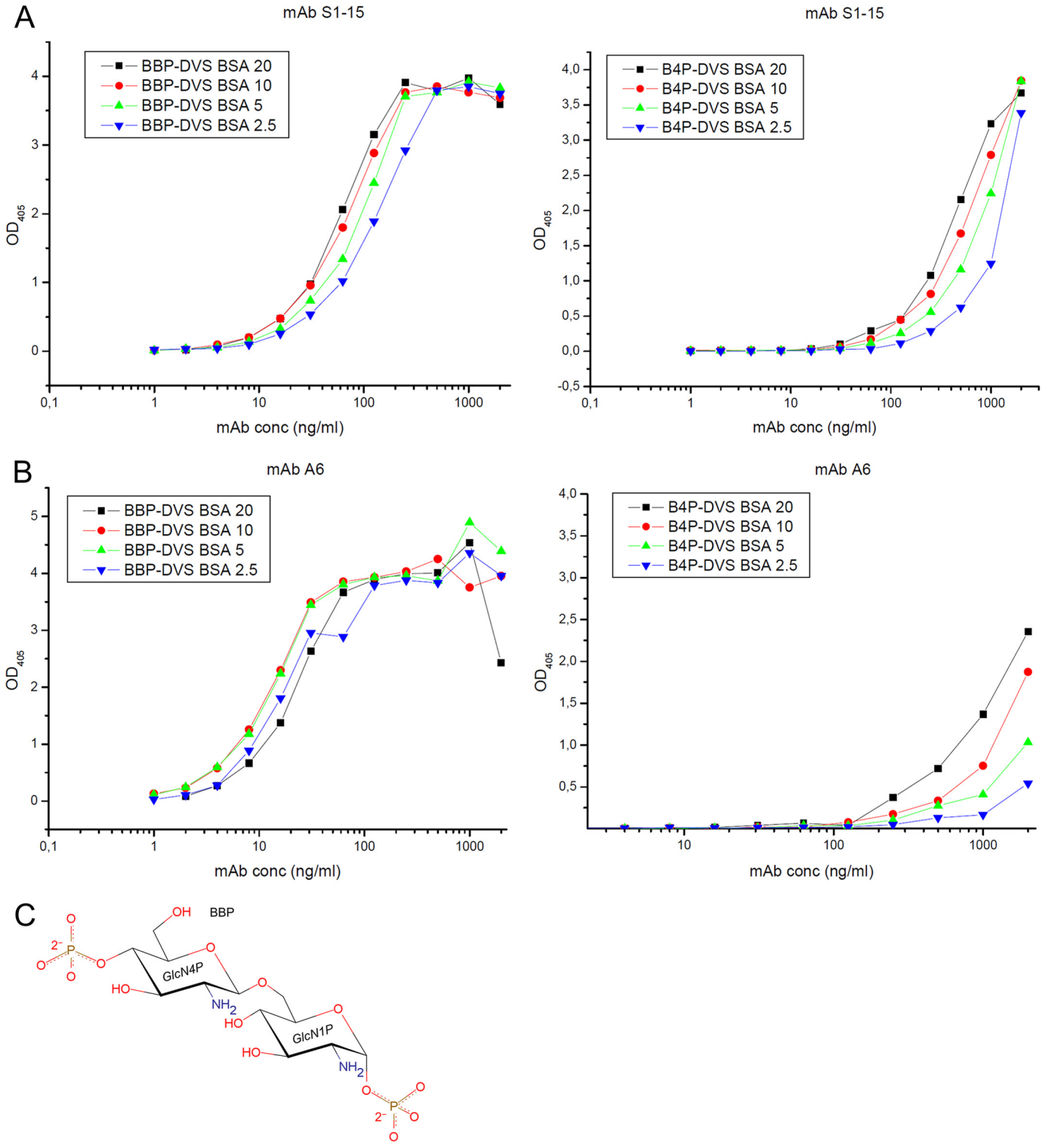

FIGURE 1. Quantitative conjugate ELISAs coated with graded concentrations of neoglycoconjugates corresponding to 2.5 (*blue triangle*), 5 (*green triangle*), 10 (*red circle*), and 20 (*black square*) pmol of ligand per well and reacted with mAbs (*A*) S1–15 and (*B*) A6 at concentrations indicated on the *x* axis are shown. Ligands used were bisphosphorylated lipid A backbone conjugated to BSA (BBP-divinyl sulfone BSA, *left panel*) and 4′-monophosphorylated lipid A backbone conjugated to BSA (*right panel*), and absorbance was measured at 405 nm. The chemical structure of the carbohydrate backbone of lipid A (BBP) used for crystallization trials (*C*). *1P* and *4P* refer to the position of the phosphates on the pyranose ring.

of a Ser(H)-94 to Arg (residues are identified as H or L to denote the heavy chain and light chains, respectively) at the base of CDR H3. The D- and J-genes of S1–15 are identical in nucleotide sequence to their respective germ line genes IGHD2–1*01 and IGHJ3*01. The A6 V_H chain V-, D-, and J-genes belong to IGHV5–6-2*01, IGHD2–1*01, and IGHJ4*01, respectively. The V-, D-, and J-genes of A6 share 280/288, 40/42, and 43/50 in nucleotide identity with their respective germ line genes. Overall, there are 16 amino acid mutations from the germ line gene in A6, six of which lie in the CDRs;

TABLE 1
Data collection and refinement statistics for liganded and unliganded structures of lipid A-specific antibodies, A6 and S1–15

	Crystal					
	S1–15 BBP	**S1–15 unliganded**	**A6 BBP**	**A6 unliganded**	**S1–15 T5[a]**	**S1–15 T5 no 5′*P*[a]**
PDB codes	4ODT	4ODU	4ODV	4ODW	4Z8F	4Z95
Resolution (Å)	25.0-1.95 (2.02-1.95)	30.00-2.29 (2.34-2.29)	25.0-2.15 (2.23-2.15)	25.0-2.70 (2.80-2.70)	25.0-1.75 (1.81-1.75)	30.00-1.79 (1.85-1.79)
Space group	$P4_32_12$	$P2_1$	$P2_12_12_1$	$P1$	$P4_32_12$	$P4_32_12$
a (Å)	77.5	75.8	37.6	42.1	77.6	77.8
b (Å)	77.5	77.6	64.3	69.2	77.6	77.8
c (Å)	156.2	72.0	154.2	69.1	156.3	156.5
α (°)	90.0	90.0	90.0	71.0	90.0	90.0
β (°)	90.0	96.8	90.0	72.4	90.0	90.0
γ (°)	90.0	90.0	90.0	88.3	90.0	90.0
Volume Å^3	937500	420390	372247	180558	940639	946473
Wavelength (Å)	0.979	0.979	0.979	0.979	0.979	0.979
Mean *B*-factor (Å^2)	40.3	31.0	48.1	53.30	38.9	39.0
Z	1	2	1	2	1	1
Unique reflections	35,329	34,731	21,015	18,489	46,712	43,755
Redundancy	15.7 (15.8)	5.0 (5.1)	4.9 (4.5)	2.0 (2.0)	14.5 (14.5)	9.9 (10.0)
$\langle I/\sigma(I)\rangle$	34.1 (4.91)	24.4 (2.79)	16.0 (4.13)	18.2 (1.86)	36. 0 (5.95)	37.7 (3.7)
R_{sym} (%)	8.8 (78.6)	6.3 (61.5)	8.5 (40.4)	4.0 (47.2)	5.90 (61.0)	5.3 (74.0)
Completeness (%)	100.0 (100.0)	100.0 (100.0)	99.7 (99.1)	98.1 (98.3)	99.9 (100.0)	99.9 (100.0)
Protein atoms	3375	6662	3338	6534	3375	3375
Solvent atoms	265	300	94	16	208	278
Heterogen[b] atoms	64	10	38	8	101	5
Nucleic acids	0	0	0	0	5	0
Ramachandran outliers	0	1	3	0	0	0
Solvent content (%)	49.0	44.9	36.8	37.3	48.4	49.9
Refinement						
R_{work} (%)	19.7	18.7	20.4	23.1	20.8	20.3
R_{free} (%)	22.4	23.3	24.9	25.7	24.0	23.6
r.m.s. bond lengths (Å)	0.0091	0.010	0.011	0.011	0.0093	0.010
r.m.s. bond angles (°)	1.33	1.42	1.56	1.61	1.28	1.34

[a] Antigen T5 represents the DNA oligonucleotide 5′*P*-TTTTT-3′*P*.
[b] Heterogen atoms describe nonstandard residues, such as prosthetic groups, inhibitors, carbohydrates, solvents, and ions.

there were only five amino acid mutations away from the germ line in S1–15 with only one in the combining site (Table 2).

A6 Recognition of Lipid A—There are 11 direct hydrogen bonds to the bisphosphorylated lipid A backbone BBP and two bridging water interactions from one water molecule (Fig. 2*E* and Table 3). There are three salt bridge interactions as follows: a bidentate salt bridge between 1*P* and Arg(H)-100A and a bifurcated salt bridge between 1*P* and Arg(L)-30. An additional contact is formed with the 1*P* through Tyr(L)-32. Tyr(L)-32 also shares a hydrogen bond with the ring oxygen of the first GlcN. The 4*P* forms two hydrogen bonds with Tyr(H)-96 and Tyr(L)-49 hydroxyl groups and a salt bridge with Lys(L)-53 residue. The final two hydrogen bonds stem from the terminal GlcN ring oxygen and C6 hydroxyl to Asn(H)-98 and His(H)-100C, respectively. Tyr(L)-50 forms multiple hydrophobic contacts (data not shown) with the hydrophobic face of the terminal GlcN, and an additional strong hydrophobic contact (3.45 Å) to the C6 of the first GlcN residue (Fig. 2*E*, *dashed lines*).

S1–15 Recognition of Lipid A—There are eight direct hydrogen bond contacts to the BBP and six bridging water interactions from four water molecules (Fig. 2*F* and Table 3). There are two salt bridge interactions as follows: a bidentate salt bridge between 4-phosphate (4*P*) and Arg(H)-52 and salt bridge between 4*P* and Arg(H)-96. There are also two additional weak electrostatic interactions as follows: one between 4*P* and Arg(H)-50 and another between 1*P* and Arg(H)-94 at a distance of 4.07 and 3.96 Å, respectively. The backbone amide of Ala(H)-33 and the backbone oxygen of Arg(H)-96 both participate in hydrogen bonds with the C6 hydroxyl of the β-GlcN (GlcN4*P*). A second backbone amide of Ala(H)-98 forms a hydrogen bond to the ring oxygen on the α-GlcN. The 1*P* group forms two hydrogen bonds with a side chain of Tyr(H)-32 and Tyr(H)-100B residues. Finally, there is a hydrophobic interaction (~3.7 Å) between the Tyr(H)-32 phenyl ring and the C6 methyl group on the α-GlcN (Fig. 2*F*, *dashed lines*).

Comparison with DNA-specific Antibodies—The *V*-genes of numerous DNA-specific antibodies have been determined (35, 51–53), many of which belong to five subgroups of the J558 family as follows: V_H238 (IGHV5-9-03 or 01*),[4] 133.16V_H (IGHV1–82-01*), V_H31 (IGHV1S19–01*), 6G6V_H (IGHV7–3-04*), and pH3–6a (IGVH9–1-02*). Various antibodies utilizing these genes have been reported to be involved in polyspecificity to *p*-azophenylarsenate (54), cardiolipin (52), and other autoantigens (55). The *V*-genes of mAb A6 are closely related to several characterized anti-DNA mAbs (51, 52). The V_L chain genes of A6 and S1–15 share over 90% nucleotide identity with several anti-DNA antibodies (52). One of the closest examples include an antibody isolated from hybridoma cell line 73.23 (52) with 96/108 amino acid sequence identity. Although the V_H chain *V*-gene of A6 is not involved in the recognition of lipid A antigen, it is closely related to known anti-DNA *V*-gene known as V_H238 (51), sharing 273/291 nucleotides and 85/98 amino acids.

S1–15 also shares V_H genes with an ssDNA-specific autoantibody, BV04-01 (56), and is closely related to antibody Dna-1 (57). S1–15 shares 92% amino acid sequence identity with BV04-01 on the V_H chain, although they do not share V_L chain

[4] The gene designations shown in parentheses are based on the IMGT/V-quest database (Monod *et al.* (41) and Brochet *et al.* (40)) and are used throughout this paper.

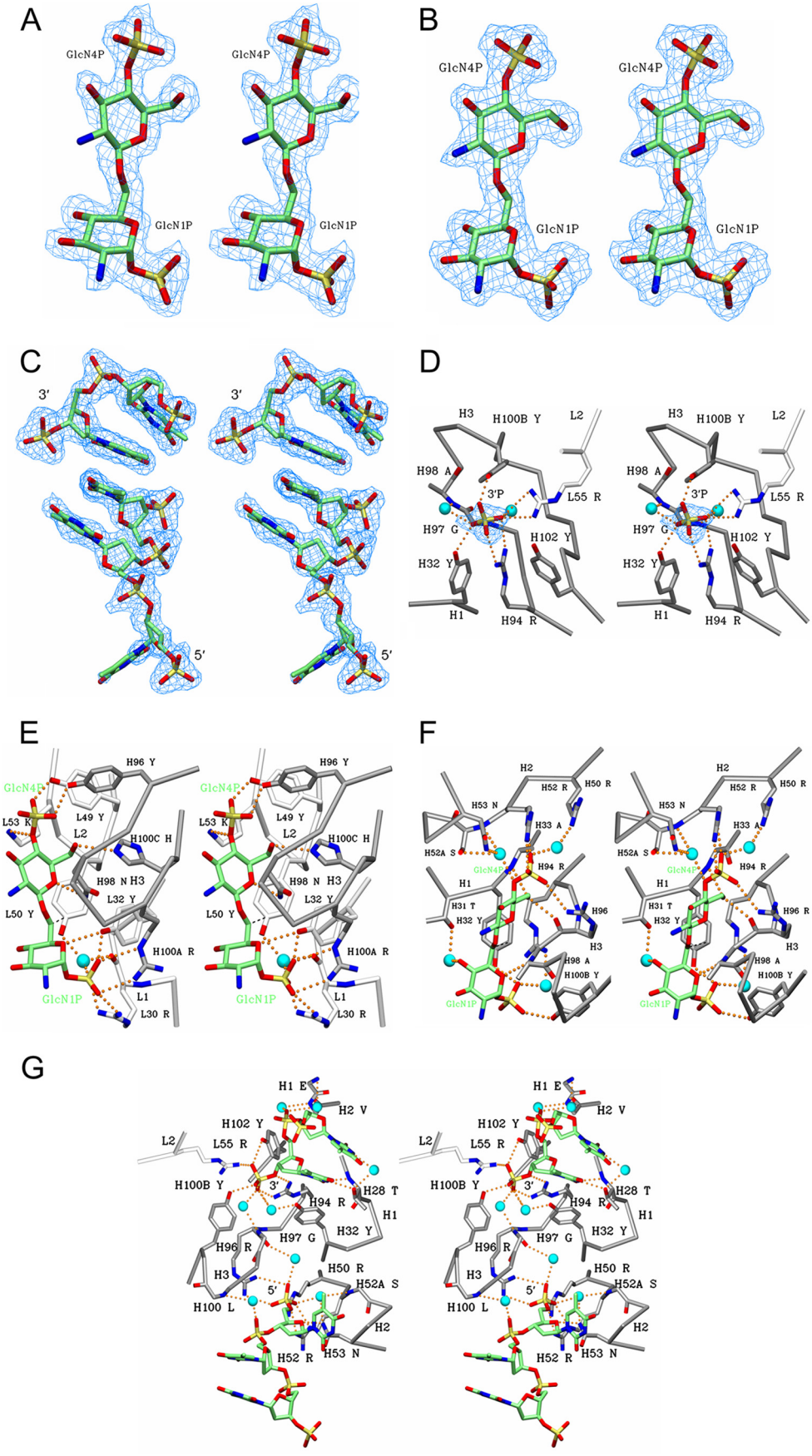
A
GlcN4P
GlcN1P
GlcN4P
GlcN1P
B
GlcN4P
GlcN1P
GlcN4P
GlcN1P
C
3′
5′
3′
5′
D
H3
H100B Y
L2
H98 A
3′P
L55 R
H97 G
H102 Y
H32 Y
H1
H94 R
H3
H100B Y
L2
H98 A
3′P
L55 R
H97 G
H102 Y
H32 Y
H1
H94 R
E
H96 Y
GlcN4P
L53 K
L49 Y
L2
H100C H
H98 N H3
L32 Y
L50 Y
H100A R
GlcN1P
L1
L30 R
H96 Y
GlcN4P
L53 K
L49 Y
L2
H100C H
H98 N H3
L32 Y
L50 Y
H100A R
GlcN1P
L1
L30 R
F
H2
H52 R
H50 R
H53 N
H33 A
H52A S
GlcN4P
H94 R
H1
H31 T
H32 Y
H96
H3
H98 A
H100B Y
GlcN1P
H2
H52 R
H50 R
H53 N
H33 A
H52A S
GlcN4P
H94 R
H1
H31 T
H32 Y
H96 R
H3
H98 A
H100B Y
GlcN1P
G
H1 E
H2 V
H102 Y
L2
L55 R
H100B Y
3′
H28 T
H94 R
H1
H32 Y
H97 G
H96 R
H3
H50 R
5′
H52A S
H100 L
H2
H52 R
H53 N
H1 E
H2 V
H102 Y
L2
L55 R
H100B Y
3′
H28 T
H94 R
H1
H32 Y
H97 G
H96 R
H3
H50 R
5′
H52A S
H100 L
H2
H52 R
H53 N

TABLE 2

Amino acid sequences of the CDR regions for S1–15 and A6 mAbs

The sequences of S1–15 and A6 likely originate from germ-line (GL) sequence 1 and 2, respectively. The V_L chain germ line genes of A6 originate from identical genes as that of S1–15. Numbering is based on the Kabat scheme. Underlined amino acids indicate residues mutated from the germ line, and residues in boldface are contacting the lipid A antigen either directly or through water bridges.

Variable Light Chain (V_L)

Clone	10	20	26 ABCDEF	32	40	49	56
S1-15	DIQMTQSTSS	LSASLGDRVT	ISCRAS	Q------DISNY	LNWYQQKP	DGTVKVLIY	YTSRLRS
GL1	DIQMTQTTSS	LSASLGDRVT	ISCRAS	Q------DISNY	LNWYQQKP	DGTVKLLIY	YTSRLHS
A6	DIVLTQSTSS	LSASLGDRVT	ITCRAS	Q------DIRNY	LSWYQQRP	DGTVKLLIY	YTSKLHS
GL2	DIQMTQTTSS	LSASLGDRVT	ISCRAS	Q------DISNY	LNWYQQKP	DGTVKLLIY	YTSRLHS
				<--CDR L1-->			<-CDR L2->

Clone	60	70	80	87 AB 98		107
S1-15	GVPS RFSGSGSGTD	YSLTISNLEQ	EDIATYF	CQQGNTLP--	WTF	GGGTKLEIK
GL1	GVPS RFSGSGSGTD	YSLTISNLEQ	EDIATYF	CQQGNTLP--	WTF	GGGTKLEIK
A6	GVPS RFSGSGSGTD	YSLTITNLEQ	EDIATYF	CQQGKTLPL-	YTF	GGGTKLEIK
GL2	GVPS RFSGSGSGTD	YSLTISNLEQ	EDIATYF	CQQGNTLPL-	YTF	GGGTKLEIK
				<---CDR L3--->		

Variable Heavy Chain (V_H)

Clone	10	20	25	35	40	49 ABC 62
S1-15	EVKLVESGGG	LVQPKGSLKL	SCAAS GFTFNTYAMN	WVRQA	PGKGLEWVA	RIRSKSNNYATYYADS
GL1	EVQLVESGGG	LVQPKGSLKL	SCAAS GFTFNTYAMN	WVRQA	PGKGLEWVA	RIRSKSNNYATYYADS
A6	EVKLVESGGG	LVKLGGSLKL	SCAAS GFTFSSYYMS	WVRQT	PEKRLELVA	AINS--NGGNTYYPDT
GL2	DVKLVESGGG	LVKLGGSLKL	SCAAS GFTFSSYYMS	WVRQT	PEKRLELVA	AINS--NGGSTYYPDT
			<-CDR H1->			<----CDR H2---->

Clone	70	80 ABC	92	ABCDEFGH 101	112
S1-15	VKDRFTIS	RDDSQSMLYL	QMNNLKTEDTAMYYC	VRHRGAPLYYGNGAWF--A	YWGQGTLVTVS
GL1	VKDRFTIS	RDDSQSMLYL	QMNNLKTEDTAMYYC	VSHRGAPLYYGNGAWF--A	YWGQGTLVTVS
A6	VKGLFTIS	RDNAKNTLYL	QMSRLKSEDTALYYC	TRLYGNYVRIHTM-----D	YWGQGTSVTVS
GL2	VKGRFTIS	RDNAKNTLYL	QMSSLKSEDTALYYC	ARLYGNYVRIHAM-----D	YWGQGTSVTVS
				<------CDR H3------>	

genes nor do their heavy chain *V*-genes match any of the five known anti-DNA *V*-gene subtypes. Conversely, S1–15 only shares 51% sequence identity with Dna-1 V_H chain, but many of these differences are conservative substitutions. Only one of the critical residues contacting lipid A is not present in Dna-1, namely Arg(H)-96.

S1–15 Recognition of ssDNA—The crystal structure of S1–15 Fab in complex with *p*5(dT)*p* showed two different oligonucleotide fragments bound at each phosphate-binding site, with a total of 14 hydrogen bonds between ssDNA ligands (Table 3) and residues of the combining site. These include five salt bridges to the terminal phosphates, and 12 hydrogen bonds mediated by eight water molecules (Fig. 2*G*). There are three salt bridges to the 5′*P*, formed via Arg(H)-50, Arg(H)-52, and Arg(H)-96. The two latter residues form a bidentate salt bridge. There are also two additional electrostatic interactions to the 3′-terminal phosphate as follows: a bidentate salt bridge from Arg(H)-94 and salt bridge from Arg(L)-55. Tyr(H)-100B and Tyr(H)-102 residues are involved in the hydrogen bonding to the terminal 3′-phosphate. There are only two hydrogen bonds formed between thymidine bases of the ssDNA fragments and the antibody-combining site, both from Thr(H)-28 to the thymidine on the 3′-terminal end. One hydrogen bond is also formed between the ring oxygen of the deoxyribose moiety on

FIGURE 2. Stereo diagram $2F_o - F_c$ electron density map (*blue*) contoured at 1.0σ for the BBP lipid A analogue was observed in the combining sites of A6 (*A*) and S1–15 mAbs (*B*) and two single-stranded DNA fragments. *p*2(dT)*p* (*top*) and *p*3(dT)*p* (*bottom*) were observed in the combining site of S1–15 (*C*). To show the base stacking interaction, the trinucleotide (*bottom*) is bound to a symmetry-related Fab. Although the original antigen used was *p*5(dT)*p*, only two and three nucleotides could be modeled with confidence. Stereo diagram of S1–15 in complex with 5(dT)*p* ligand showing hydrogen bonds (*orange dashed spheres*) between residues of S1–15 and to the 3′*P* (*D*). The remainder of the antigen was disordered. Indirect hydrogen bonds mediated by waters (*cyan spheres*) are also shown. CDR loops of the light and heavy chain are colored *white* and *gray*, respectively. Color scheme is as follows: carbon, *green*; oxygen, *red*; nitrogen, *blue*; phosphorus, *orange*; water, *cyan*. Density (*blue*) for the phosphate is contoured at 1.0σ. Stereo view of A6 (*E*) and S1–15 (*F*) in complex with lipid A analogues BBP shows hydrogen bonds and water bridges between the antigen and S1–15. CDR loops of the light and heavy chain are colored *white* and *gray*, respectively. Strong hydrophobic contacts are shown as *dashed lines* (*black*). C6 hydroxyl group of second GlcN is the attachment point to inner core residues of LPS. Stereo diagram of S1–15 Fab in complex with two *p*5(dT)*p* ssDNA fragments is shown (*G*). Stereo diagram of S1–15 Fab in complex with two *p*5(dT)*p* ssDNA fragments is shown.

TABLE 3

Hydrogen bond interactions between mAbs A6 and S1–15 to lipid A BBP and between S1–15 and oligonucleotide ligand

Lipid A numbering scheme is given in Fig. 2*A*. The distance cutoff for hydrogen bond assignment was 3.3 Å, except for charged residue interactions where the distance cutoff was 3.9 Å. Asterisk indicates charged residue interaction.

Antibody and PDB code	Antigen		Antibody		CDR	Distance
	Residue	Atom(s)	Residue	Atom		
						Å
A6 4ODV	GlcN4*P*	O6	His(H)-100C	NE2	H3	3.04
		O5	Asn(H)-98	ND2	H3	3.16
		$4PO_4$	Tyr(H)-96	OH	H3	2.68
			Lys(L)-53	NZ	L2	3.33*
			Tyr(L)-49	OH	L2	2.46
	GlcN1*P*	O5	Tyr(H)-32	OH	H1	3.15
		$1PO_4$	Tyr(H)-32	OH	H1	2.24
			Arg(H)-100A	NE	H3	3.34*
			Arg(H)-100A	NH_2	H3	2.87*
			Arg(L)-30	NH1	L1	2.41*
			Arg(L)-30	NH_2	L1	2.57*
S1–15 4ODT	GlcN4*P*	O6	Ala(H)-33	N	H1	2.95
			Arg(H)-96	O	H3	2.85
		$4PO_4$	Arg(H)-52	NE	H2	2.81*
			Arg(H)-52	NH_2	H2	2.70*
			Arg(H)-96	NH1	H3	3.09*
	GlcN1*P*	O5	Ala(H)-98	N	H3	3.06
		$1PO_4$	Tyr(H)-32	OH	H1	2.62
			Tyr(H)-100B	OH	H3	2.52
S1–15 4Z8F	dT chain E	$3'PO_4$	Arg(H)-94	NH1	H3	2.96*
			Arg(H)-94	NH_2	H3	2.69*
			Tyr(H)-100B	OH	H3	2.68
			Tyr(H)-102	OH	H3	3.12
			Arg(L)-55	NH_2	L2	2.71*
		O^2	Thr(H)-28	N	H1	2.85
		N3	Thr(H)-28	OG1	H1	2.88
	dT chain A	$5'PO_4$	Arg(H)-50	NH1	H3	2.39*
			Arg(H)-50	NH1	H3	2.91*
			Arg(H)-52	NE	H3	2.92*
			Arg(H)-52	NH_2	H3	2.87*
			Arg(H)-96	NH1	H3	3.05*
			Arg(H)-96	NH_2	H3	2.93*
		O5	Asn(H)-53	ND2	H2	2.99
		O2	Ser(H)-52	OG	H2	3.06[a]

[a] Poor electron density was observed for the terminal thymidine of chain A, and this hydrogen bond therefore cannot be assigned with confidence.

the 5′-terminal end and Asn(H)-53. Finally, there are several hydrophobic interactions between Pro(H)-99 ring carbons and the 5′-terminal thymidine base (data not shown).

Crystallization of S1–15 with an ssDNA oligomer lacking the 5′-terminal phosphate resulted in the occupancy of only one phosphate-binding site. Density could only be observed for the terminal 3′*P* (Fig. 2*D*), with many of the same residues forming contacts to the 3′-phosphate as with the *p*5(dT)*p* complexed structure. Interestingly, the 3′*P* occupies a slightly different space, resulting in the loss of the hydrogen bond to Tyr(H)-102 and the formation of a hydrogen bond to Tyr(H)-32, rather than the water bridge observed in the *p*5(dT)*p* structure (Fig. 2*D*).

Least Square Superposition of Liganded and Unliganded Fv Structures—Least square alignments of the α-carbon backbones of the V_L chains of the corresponding liganded and unliganded Fv structures of S1–15 and A6 are presented in Fig. 3, *A* and *B*. The alignment does not include the Fv structure of S1–15 in complex with oligonucleotides, because no significant changes in conformation were observed in comparison with the structure in complex with lipid A. The root mean square deviation (r.m.s.d.) between the liganded and unliganded S1–15 Fv structures are presented in the order of V_L to V_H, respectively: 0.12 and 0.31 Å for the entire Fv, including a maximum of 2.55 and 1.63 Å and a minimum of 0.02 and 0.06 Å. The only conformational change between the liganded and unliganded occurred for Ser(L)-7, which is responsible for the ~2.55 Å shift (Fig. 3*A*). The alignment of A6 resulted in a mean r.m.s.d. of 0.16 and 0.52 Å, a maximum of 1.07 and 10.7 Å, and a minimum of 0.03 and 0.12 Å for the V_L and V_H, respectively. The three different Fv molecules of A6 showed a large conformational change around Lys(H)-64 on framework region 3 (FR3), resulting in 10.7 Å r.m.s.d. observed. A significant structural shift was also observed between liganded and the two unliganded Fab molecules on CDR H3 with an r.m.s.d. of 5.02 Å (Fig. 3*B*).

Discussion

Steric Hindrance Prevents S1–15 and A6 from Binding LPS—The liganded structures for mAbs S1–15 and A6 demonstrate the structural basis for the failure of these antibodies to recognize LPS-bound lipid A (29, 58), which is the steric hindrance surrounding the C6 hydroxyl of the second GlcN residue that forms the attachment point of the inner core. Furthermore, mAbs S1–15 and A6 possess a pocket specific to the OH-6 (Fig. 3, *C* and *D*) and form a hydrogen bond to this hydroxyl. Both factors are consistent with the observed loss of binding to lipid A upon the formation of the 6-*O*-methyl derivative (29).

S1–15 and A6 Lipid A Recognition Strategy—The binding mechanism of antibodies is often described as "lock and key" or "induced fit" based on the degree of dislocation of the CDRs when comparing bound and unbound states of the antibody (16, 59–64). Comparison between the unliganded and liganded structure of S1–15 showed that lock and key type, with its associated minimum entropic penalty upon binding (Fig. 3*A*). However, mAb A6 displayed a significant degree of induced fit, particularly in the FR3 of the V_H where a maximum r.m.s.d. of 10.7 Å was observed (Fig. 3*B*).

An antibody-combining site can form a pocket or groove, or a combination of both depending on the nature of antigen recognition. Antibodies specific for proteins and larger structures often utilize grooves, although antibodies specific for oligosaccharides and haptens often utilize pockets. As expected, each of the lipid A-specific antibodies uses a pocket with high structural and charge complementarity to lipid A (Fig. 3, *C* and *D*). Carbohydrate-specific antibodies are usually observed to bind antigen along the V_L/V_H interface, which explains the difficulty that has been reported in attempts to use the phage display technique to isolate single domain antibodies (*i.e.* composed solely of a heavy or light chain variable domain) specific for carbohydrates larger than a monosaccharide (65, 66). Interestingly, the lipid A-specific antibody S1–15 Fab binds lipid A with no involvement of the light chain (Figs. 2*F* and 3*C*). Although antibodies have been observed to recognize monosaccharides in pockets formed exclusively by heavy CDRs (67), this is the only structural example to date of an antibody using a heavy chain binding pocket to bind a carbohydrate moiety larger than a monosaccharide.

Comparison between S1–15 and A6 Binding to Lipid A—Although there are similarities, the combining sites utilize strikingly different mechanisms to recognize the lipid A backbone. In contrast to S1–15, mAb A6 binds to the lipid A antigen with both V_L and V_H chain residues, despite sharing V_L chain genes with S1–15. Most of the hydrogen bonds in the S1–15·lipid A complex are directed toward the 4*P* of the second

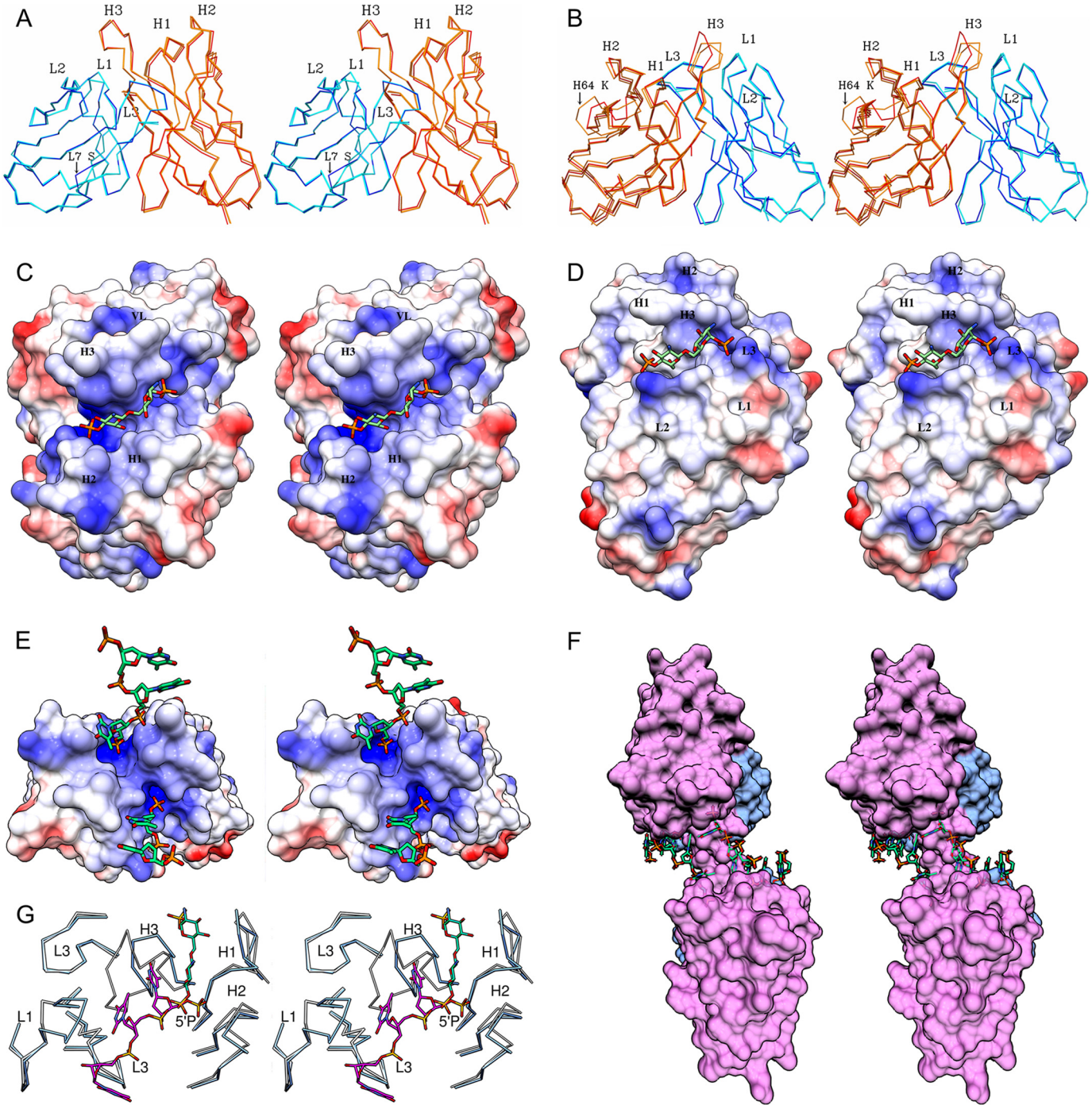

FIGURE 3. Stereo view of Fv structure alignments between liganded and unliganded structures of S1–15 (*A*) and A6 (*B*) is shown. Alignments were carried out using the α-carbon trace of the liganded V_L as the reference structure for each antibody. Displacement of CDR L1 and H3 is highlighted. *Dark blue,* liganded light chain. *Cyan,* unliganded light chains. *Orange,* unliganded heavy chains. *Red,* liganded heavy chain. Because of conformational differences, both unliganded molecules in the asymmetric unit were included in the alignment of A6. Stereo images of the electrostatic surface potentials for Fv structures of S1–15 (*C*) and A6 (*D*), bound to lipid A analogue. *Blue regions* represent relatively positive surface charge, and *red* represents negative surface charge. *White* represents neutral surface charge. α-Carbon alignment between BV04-01 Fv (*blue*) and S1–15 Fv (*white*) in complex with a trinucleotide (*khaki*) and lipid A (*green*), respectively (*E*), is shown. Transparent surface diagram showing S1–15 Fv and symmetry-related Fv molecule in complex with *p*5(dT)*p* (*green*) fragments (*F*) is shown. The V_L and V_H domains are colored *blue* and *pink,* respectively. Stereo images of the electrostatic surface potentials for S1–15 Fv in complex with *p*5(dT)*p* ssDNA fragments. The lipid A 4′*P* binding pocket of S1–15 is closely related to the 5′*P*-binding site of BV04-01. For clarity, only the α-carbon trace of the CDRs is shown for each antibody (*G*).

GlcN (Fig. 2*F*), complementing ELISA data, where binding toward the 4*P*-monophosphorylated lipid A antigen is largely retained (Fig. 1*A*). A6 forms multiple contacts through both V_L and V_H chain residues to both phosphates of the lipid A analogue BBP, with the majority of these contacts directed toward the 1*P* (Fig. 2*E*), and thus there is a significant loss of avidity to the 4*P*-monophosphorylated lipid A (Fig. 1*B*). One feature common to both antibodies is a strong hydrophobic contact between the C6 carbon of the first GlcN (Fig. 2, *E* and *F*, *dashed lines*) and Tyr residues His-32 and Leu-50.

From the conjugate ELISA, we determined the relative strength of binding, showing a 64-fold increase in avidity toward the bisphosphorylated lipid A backbone when comparing A6 to S1–15 at 2 pmol/well concentration of antigen (Fig. 1, *A* and *B*). This trend is consistent with the number of contacts and salt bridges formed between these antibodies and lipid A. A6 forms 11 hydrogen bonds, three of which are charged interactions. In contrast, S1–15 forms eight hydrogen bonds between lipid A and residues of S1–15, two of which are charged residue interactions.

Sequence Comparison to Anti-nucleotide Antibodies and the Basis for Polyspecificity—The structure of A6 and S1–15 in complex with lipid A carbohydrate backbone revealed distances of 11.9 and 12.1 Å, respectively, between the 1′- and 4′-phosphates, which approximate the distance (11.1 Å) observed in the trinucleotide in complex with antibody BV04-01 Fab.

Similarities in sequence had pointed toward potential polyspecificity of A6 and S1–15 toward ssDNA, as antibodies produced by immunization with lipid A carbohydrate backbone often share *V*-genes with DNA-specific antibodies. For example, the antibody belonging to the hybridoma cell line 73.23 possesses a related V_L gene to A6 mAb, which not only binds ssDNA but dsDNA with lower avidity (52). Of the residues contacting lipid A for mAb A6, only Arg(L)-30 differs from anti-DNA antibody 73.23 (replaced by Ser(L)-30). Although the heavy chain V-region (coded by the *V*-gene) of A6 is not involved in recognition of lipid A, the regions corresponding to the *D* and *J* genes of CDR H3 play a crucial role. DNA-specific antibodies have been shown to have CDR H3 loops dominated by Arg and Tyr residues (51), which is a feature shared with the CDR H3 of A6 (Table 2).

Structural Basis for S1–15 ssDNA Polyspecificity—Crystals were observed growing in number of different conditions, and several structures determined where the oligonucleotide was highly disordered (data not shown). After considerable optimization over a large range of different conditions and ligands, a structure with interpretable density was obtained for S1–15 in complex with the 5(dT) oligonucleotide; however, the combining site was not spanned by a single molecular ssDNA, but it bound two separate oligonucleotides by their terminal 5′- and 3′-phosphate groups (Fig. 3*E*). This arrangement was stabilized by base stacking between symmetry-related oligonucleotides (Figs. 2*C* and 3*F*). The phosphate binding pocket on S1–15 that recognizes 1*P* of lipid A binds the terminal 3′-phosphate, although the 4*P* lipid A pocket binds the 5′-phosphate. Interestingly, higher temperature factors were observed for the 5′-terminal phosphate-binding site when refined at full occupancy, despite the fact that there are more interactions with the 5′*P*. This appears to be due to two reasons. First there are two base-specific hydrogen bonds out of the total 14, both occurring at the 3′-terminal end. Second, the 3′-terminal thymidine base formed stacking interactions with the neighboring thymidine nucleotide. Furthermore, in the S1–15 Fab structure in complex with the 5(dT)*p* (lacking 5′*P*), density is only observable for the 3′-terminal phosphate with the residual oligonucleotides being disordered. This suggests that the 5′*P*-binding site plays a crucial role in stabilizing the second oligonucleotide fragment via stacking interactions on the 3′*P*-binding site.

Finally, density for the thymidine base on the 5′ end was poor in the *p*5(dT)*p* liganded structure due to high thermal motion, consistent with the lack of stabilizing stacking interactions.

Structural Comparison with Single-stranded Nucleotide-specific Antibodies—Published anti-ssDNA antibody structures show that the backbone phosphates are usually oriented away from the combining site, with the CDRs interacting directly through stacking interactions with the hydrophobic bases.

Autoantibody BV04-01 does recognize the backbone phosphate groups in its complex with the trinucleotide *p*5(dT) (lacking the 3′*P*), with the central thymidine forming stacking interactions with a Tyr and a Trp residue on either side of the thymidine (56). Additionally, the 5′*P* and central phosphate groups of the trinucleotide contribute to binding through hydrogen bonds, and interestingly, the 5′*P*-binding site of BV04-01 contains many interactions that correspond to the 5′*P* (and the 4′*P* lipid A)-binding site of S1–15 (Fig. 3*G*), marking its importance for dual recognition of ssDNA and lipid A. Of the three phosphates of the trinucleotide bound to BV04-01, only one phosphate formed a salt bridge to the Fab.

Similarly the RNA-specific antibody Jel 103 Fab structure in complex with RNA nucleotide (Protein Data Bank code 1MRF) display base stacking interaction with a Tyr residue and two salt bridges to the phosphate moiety from Lys and Arg residues, respectively (47).

It is remarkable that S1–15 and A6 bind ssDNA at all, as both have undergone affinity maturation toward the lipid A carbohydrate antigen, and the corresponding germ line antibodies could exhibit alternative binding modes to ssDNA than observed here. Crucially, the higher avidity of decavalent IgM plays an important role in establishing polyspecificity toward single-stranded nucleic acids. Binding assays have shown significant binding to various ssDNA fragments for both antibodies (data not shown), and additional crystallization studies with these antigens are ongoing.

Conclusions—The structures of mAbs S1–15 and A6 provide a structural explanation of their inability to bind intact LPS.

The ability of antibodies to undergo somatic hypermutation implies that germ line antibodies in general must display a significant degree of cross-reactivity or polyspecificity to increase the number of antigens recognized. Although there has been significant progress toward structural characterization of antibody cross-reactivity, there is a dearth of structures demonstrating the polyspecific nature of antibodies. These structures show significant binding to terminal nucleotides and shorter ssDNA oligonucleotides via positively charged surface complementary to the terminal phosphates. Structural insights into the molecular basis for polyspecificity against ssDNA is of clinical interest and may provide crucial clues into how these antibodies arise as implicated in autoimmune diseases such as systemic lupus erythematosus, thyroiditis, and rheumatic autoimmune diseases.

Author Contributions—O. H. G. performed the experiments shown in Figs. 2 and 3, conceived some of the experiments, analyzed the data, and wrote a major part of the paper. S. M. L. performed the ELISA experiments shown in Fig. 1, conceived some of the experiments, analyzed the data, and contributed to the paper. T. R. performed some of the experiments. L. B. performed some of the experiments, analyzed the data, and contributed to the paper. P. K. provided reagents and contributed to the paper. H. B. provided reagents, conceived many of the experiments, and contributed to the paper. S. V. E. conceived many of the experiments and wrote a major part the paper. All authors reviewed the results and approved the final version of the manuscript.

Acknowledgments—We gratefully acknowledge the technical assistance of Ute Agge, Veronika Susott, and Christine Schneider at the Research Center Borstel, Germany. Research described in this paper was performed at the Canadian Light Source, which is supported by the Canada Foundation for Innovation, Natural Sciences and Engineering Research Council of Canada, the University of Saskatchewan, the Government of Saskatchewan, Western Economic Diversification Canada, the National Research Council Canada, and the Canadian Institutes of Health Research.

References

1. Angus, D. C., Linde-Zwirble, W. T., Lidicker, J., Clermont, G., Carcillo, J., and Pinsky, M. R. (2001) Epidemiology of severe sepsis in the United States: Analysis of incidence, outcome, and associated costs of care. *Crit. Care Med.* **29,** 1303–1310
2. Engel, C., Brunkhorst, F. M., Bone, H. G., Brunkhorst, R., Gerlach, H., Grond, S., Gruendling, M., Huhle, G., Jaschinski, U., John, S., Mayer, K., Oppert, M., Olthoff, D., Quintel, M., Ragaller, M., *et al.* (2007) Epidemiology of sepsis in Germany: results from a national prospective multicenter study. *Intensive Care Med.* **33,** 606–618
3. Martin, G. S. (2012) Sepsis, severe sepsis and septic shock: changes in incidence, pathogens and outcomes. *Expert Rev. Anti.-Infect. Ther.* **10,** 701–706
4. Buttenschoen, K., Radermacher, P., and Bracht, H. (2010) Endotoxin elimination in sepsis: physiology and therapeutic application. *Langenbeck. Arch. Surg.* **395,** 597–605
5. Miller, S. I., Ernst, R. K., and Bader, M. W. (2005) LPS, TLR4 and infectious disease diversity. *Nat. Rev. Microbiol.* **3,** 36–46
6. Kim, H. M., Park, B. S., Kim, J. I., Kim, S. E., Lee, J., Oh, S. C., Enkhbayar, P., Matsushima, N., Lee, H., Yoo, O. J., and Lee, J. O. (2007) Crystal structure of the TLR4-MD-2 complex with bound endotoxin antagonist eritoran. *Cell* **130,** 906–917
7. Miyake, K. (2007) Innate immune sensing of pathogens and danger signals by cell surface Toll-like receptors. *Semin. Immunol.* **19,** 3–10
8. Hold, G., and Bryant, C. (2011) in *Bacterial Lipopolysaccharides* (Knirel, Y., and Valvano, M., eds) pp. 371–387, Springer, Vienna
9. Di Padova, F. E., Brade, H., Barclay, G. R., Poxton, I. R., Liehl, E., Schuetze, E., Kocher, H. P., Ramsay, G., Schreier, M. H., and McClelland, D. B. (1993) A broadly cross-protective monoclonal-antibody binding to *Escherichia coli* and *Salmonella* lipopolysaccharides. *Infect. Immun.* **61,** 3863–3872
10. Gomery, K., Müller-Loennies, S., Brooks, C. L., Brade, L., Kosma, P., Di Padova, F., Brade, H., and Evans, S. V. (2012) Antibody WN1 222-5 mimics Toll-like receptor 4 binding in the recognition of LPS. *Proc. Natl. Acad. Sci. U.S.A.* **109,** 20877–20882
11. Müller-Loennies, S., Brade, L., and Brade, H. (2007) Neutralizing and cross-reactive antibodies against enterobacterial lipopolysaccharide. *Int. J. Med. Microbiol.* **297,** 321–340
12. Brade, L., and Brade, H. (1985) Characterization of two different antibody specificities recognizing distinct antigenic determinants in free lipid A of *Escherichia coli*. *Infect. Immun.* **48,** 776–781
13. Fujihara, Y., Bogard, W. C., Lei, M. G., Daddona, P. E., and Morrison, D. C. (1993) Monoclonal anti-lipid A IgM antibodies HA-1A and E-5 recognize distinct epitopes on lipopolysaccharide and lipid A. *J. Infect. Dis.* **168,** 1429–1435
14. Helmerhorst, E. J., Maaskant, J. J., and Appelmelk, B. J. (1998) Anti-lipid A monoclonal antibody centoxin (HA-1A) binds to a wide variety of hydrophobic ligands. *Infect. Immun.* **66,** 870–873
15. Kuhn, H. M. (1993) Cross-reactivity of monoclonal antibodies and sera directed against lipid A and lipopolysaccharides. *Infection* **21,** 179–186
16. Blackler, R. J., Müller-Loennies, S., Brade, L., Kosma, P., Brade, H., and Evans, S. V. (2012) in *Anticarbohydrate Antibodies: From Molecular Basis to Clinical Application* (Kosma, P., and Müller-Loennies, S., eds) pp. 75–120, Springer, Vienna
17. Rynkiewicz, M. J., Lu, Z., Hui, J. H., Sharon, J., and Seaton, B. A. (2012) Structural analysis of a protective epitope of the *Francisella tularensis O*-polysaccharide. *Biochemistry* **51,** 5684–5694
18. Vulliez-Le Normand, B., Saul, F. A., Phalipon, A., Bélot, F., Guerreiro, C., Mulard, L. A., and Bentley, G. A. (2008) Structures of synthetic O-antigen fragments from serotype 2a *Shigella flexneri* in complex with a protective monoclonal antibody. *Proc. Natl. Acad. Sci. U.S.A.* **105,** 9976–9981
19. Cygler, M., Rose, D. R., and Bundle, D. R. (1991) Recognition of a cell-surface oligosaccharide of pathogenic *Salmonella* by an antibody Fab fragment. *Science* **253,** 442–445
20. Ianaro, A., Tersigni, M., and D'Acquisto, F. (2009) New insight in LPS antagonist. *Mini-Rev. Med. Chem.* **9,** 306–317
21. Li, J., Carr, B., Goyal, M., and Gaieski, D. F. (2011) Sepsis: the inflammatory foundation of pathophysiology and therapy. *Hosp. Pract.* **39,** 99–112
22. Cross, A. S. (2014) Anti-endotoxin vaccines: Back to the future. *Virulence* **5,** 219–225
23. Holst, O. (2007) The structures of core regions from enterobacterial lipopolysaccharides–an update. *FEMS Microbiol. Lett.* **271,** 3–11
24. Pollack, M., Ohl, C. A., Golenbock, D. T., Di Padova, F., Wahl, L. M., Koles, N. L., Guelde, G., and Monks, B. G. (1997) Dual effects of LPS antibodies on cellular uptake of LPS and LPS-induced proinflammatory functions. *J. Immunol.* **159,** 3519–3530
25. Kuhn, H. M., Brade, L., Appelmelk, B. J., Kusumoto, S., Rietschel, E. T., and Brade, H. (1992) Characterization of the epitope specificity of murine monoclonal antibodies directed against lipid A. *Infect. Immun.* **60,** 2201–2210
26. Galanos, C., Lüderitz, O., and Westphal, O. (1971) Preparation and properties of antisera against the lipid A component of bacterial lipopolysaccharides. *Eur. J. Biochem.* **24,** 116–122
27. Appelmelk, B. J., Verweij-van Vught, A. M., Maaskant, J. J., Schouten, W. F., De Jonge, A. J., Thijs, L. G., and Maclaren, D. M. (1988) Production and characterisation of mouse monoclonal antibodies reacting with the lipopolysaccharide core region of Gram-negative bacilli. *J. Med. Microbiol.* **26,** 107–114
28. Brade, L., Holst, O., and Brade, H. (1993) An artificial glycoconjugate containing the bisphosphorylated glucosamine disaccharide backbone of lipid-A binds lipid-A monoclonal antibodies. *Infect. Immun.* **61,** 4514–4517
29. Brade, L., Engel, R., Christ, W. J., and Rietschel, E. T. (1997) A nonsubstituted primary hydroxyl group in position 6′ of free lipid A is required for binding of lipid A monoclonal antibodies. *Infect. Immun.* **65,** 3961–3965
30. Bhat, N. M., Bieber, M. M., Chapman, C. J., Stevenson, F. K., and Teng, N. N. (1993) Human antilipid A monoclonal antibodies bind to human B cells and the I antigen on cord red blood cells. *J. Immunol.* **151,** 5011–5021
31. Miller, J. J., 3rd, Bieber, M. M., Levinson, J. E., Zhu, S., Tsou, E., and Teng, N. N. (1996) V(H)4–34(V(H)4.21) gene expression in the chronic arthritides of childhood: studies of associations with anti-lipid A antibodies, HLA antigens, and clinical features. *J. Rheumatol.* **23,** 2132–2139
32. Izui, S., Kobayakawa, T., Zryd, M. J., Louis, J., and Lambert, P. H. (1977) Mechanism for induction of anti-DNA antibodies by bacterial lipopolysaccharides in mice. II. Correlation between anti-DNA induction and polyclonal antibody formation by various polyclonal B lymphocyte activators. *J. Immunol.* **119,** 2157–2162
33. Sumazaki, R., Fujita, T., Kabashima, T., Nishikaku, F., Koyama, A., Shibasaki, M., and Takita, H. (1986) Monoclonal antibody against bacterial lipopolysaccharide cross-reacts with DNA-histone. *Clin. Exp. Immunol.*

66, 103–110
34. Spellerberg, M., Chapman, C., Hamblin, T., and Stevenson, F. (1995) Dual recognition of lipid A and DNA by human antibodies encoded by the V(H)4–21 gene–a possible link between infection and lupus. *Ann. NY. Acad. Sci.* **764,** 427–432
35. Tillman, D. M., Jou, N. T., Hill, R. J., and Marion, T. N. (1992) Both IgM and IgG anti-DNA antibodies are the products of clonally selective B-cell stimulation in (Nzb × Nzw)F(1) mice. *J. Exp. Med.* **176,** 761–779
36. Robertson, C. R., and Pisetsky, D. S. (1992) Specificity analysis of antibodies to single-stranded micrococcal DNA in the sera of normal human–subjects and patients with systemic lupus-erythematosus. *Clin. Exp. Rheumatol.* **10,** 589–594
37. Ravirajan, C. T., Rowse, L., MacGowan, J. R., and Isenberg, D. A. (2001) An analysis of clinical disease activity and nephritis-associated serum autoantibody profiles in patients with systemic lupus erythematosus: a cross-sectional study. *Rheumatology* **40,** 1405–1412
38. Pedro, A. B., Romaldini, J. H., Americo, C., and Takei, K. (2006) Association of circulating antibodies against double-stranded and single-stranded DNA with thyroid autoantibodies in Graves' disease and Hashimoto's thyroiditis patients. *Exp. Clin. Endocrinol. Diabetes* **114,** 35–38
39. Kaburaki, J., Kuwana, M., Ogasawara, T., Takano, M., Funatsu, Y., and Tojo, T. (1992) Specificity of antibodies to single-stranded (ss)DNA in SLE patients with anti-phospholipid syndrome. *Keio J. Med.* **41,** 10–15
40. Brochet, X., Lefranc, M. P., and Giudicelli, V. (2008) IMGT/V-QUEST: the highly customized and integrated system for IG and TR standardized V-J and V-D-J sequence analysis. *Nucleic Acids Res.* **36,** W503–W508
41. Monod, M. Y., Giudicelli, V., Chaume, D., and Lefranc, M. P. (2004) IMGT/Junction Analysis: the first tool for the analysis of the immunoglobulin and T cell receptor complex V-J and V-D-J junctions. *Bioinformatics* **20,** 379–385
42. McCoy, A. J., Grosse-Kunstleve, R. W., Adams, P. D., Winn, M. D., Storoni, L. C., and Read, R. J. (2007) Phaser crystallographic software. *J. Appl. Crystallogr.* **40,** 658–674
43. Emsley, P., and Cowtan, K. (2004) Coot: model-building tools for molecular graphics. *Acta Crystallogr. D Biol. Crystallogr.* **60,** 2126–2132
44. Murshudov, G. N., Vagin, A. A., and Dodson, E. J. (1997) Refinement of macromolecular structures by the maximum-likelihood method. *Acta Crystallogr. D Biol. Crystallogr.* **53,** 240–255
45. Winn, M. D., Murshudov, G. N., and Papiz, M. Z. (2003) Macromolecular TLS refinement in REFMAC at moderate resolutions. *Method Enzymol.* **374,** 300–321
46. Pettersen, E. F., Goddard, T. D., Huang, C. C., Couch, G. S., Greenblatt, D. M., Meng, E. C., and Ferrin, T. E. (2004) UCSF chimera–a visualization system for exploratory research and analysis. *J. Comput. Chem.* **25,** 1605–1612
47. Pokkuluri, P. R., Bouthillier, F., Li, Y., Kuderova, A., Lee, J., and Cygler, M. (1994) Preparation, characterization and crystallization of an antibody Fab fragment that recognizes RNA: Crystal structures of native Fab and 3 Fab-mononucleotide complexes. *J. Mol. Biol.* **243,** 283–297
48. Tormo, J., Stadler, E., Skern, T., Auer, H., Kanzler, O., Betzel, C., Blaas, D., and Fita, I. (1992) 3-Dimensional structure of the Fab fragment of a neutralizing antibody to human rhinovirus serotype-2. *Protein Sci.* **1,** 1154–1161
49. Mol, C. D., Muir, A. K., Cygler, M., Lee, J. S., and Anderson, W. F. (1994) Structure of an immunoglobulin Fab fragment specific for triple-stranded DNA. *J. Biol. Chem.* **269,** 3615–3622
50. Mol, C. D., Muir, A. K., Lee, J. S., and Anderson, W. F. (1994) Structure of an immunoglobulin Fab fragment specific for poly(dG)·poly(dC). *J. Biol. Chem.* **269,** 3605–3614
51. Shlomchik, M., Mascelli, M., Shan, H., Radic, M. Z., Pisetsky, D., Marshak-Rothstein, A., and Weigert, M. (1990) Anti-DNA antibodies from autoimmune mice arise by clonal expansion and somatic mutation. *J. Exp. Med.* **171,** 265–292
52. Ibrahim, S. M., Weigert, M., Basu, C., Erikson, J., and Radic, M. Z. (1995) Light-chain contribution to specificity in anti-DNA antibodies. *J. Immunol.* **155,** 3223–3233
53. Krishnan, M. R., Jou, N. T., and Marion, T. N. (1996) Correlation between the amino acid position of arginine in VH-CDR3 and specificity for native DNA among autoimmune antibodies. *J. Immunol.* **157,** 2430–2439
54. Rathbun, G. A., Otani, F., Milner, E. C., Capra, J. D., and Tucker, P. W. (1988) Molecular characterization of the A-J-J558 family of heavy-chain variable region gene segments. *J. Mol. Biol.* **202,** 383–395
55. Monestier, M., Bonin, B., Migliorini, P., Dang, H., Datta, S., Kuppers, R., Rose, N., Maurer, P., Talal, N., and Bona, C. (1987) Autoantibodies of various specificities encoded by genes from the Vh J558 family bind to foreign antigens and share idiotopes of antibodies specific for self and foreign antigens. *J. Exp. Med.* **166,** 1109–1124
56. Herron, J. N., He, X. M., Ballard, D. W., Blier, P. R., Pace, P. E., Bothwell, A. L., Voss, E. W., Jr., and Edmundson, A. B. (1991) An autoantibody to single-stranded-DNA- comparison of the 3-dimensional structures of the unliganded Fab and a deoxynucleotide Fab complex. *Proteins* **11,** 159–175
57. Tanner, J. J., Komissarov, A. A., and Deutscher, S. L. (2001) Crystal structure of an antigen-binding fragment bound to single-stranded DNA. *J. Mol. Biol.* **314,** 807–822
58. El-Samalouti, V. T., Schletter, J., Brade, H., Brade, L., Kusumoto, S., Rietschel, E. T., Flad, H. D., and Ulmer, A. J. (1997) Detection of lipopolysaccharide(LPS)-binding membrane proteins by immuno-coprecipitation with LPS and anti-LPS antibodies. *Eur. J. Biochem.* **250,** 418–424
59. Rini, J. M., Schulze-Gahmen, U., and Wilson, I. A. (1992) Structural evidence for induced fit as a mechanism for antibody-antigen recognition. *Science* **255,** 959–965
60. Wilson, I. A., and Stanfield, R. L. (1994) Antibody-antigen interactions: new structures and new conformational-changes. *Curr. Opin. Struct. Biol.* **4,** 857–867
61. Schulze-Gahmen, U., Rini, J. M., and Wilson, I. A. (1993) Detailed analysis of the free and bound conformations of an antibody. X-ray structures of Fab 17/9 and 3 different Fab-peptide complexes. *J. Mol. Biol.* **234,** 1098–1118
62. Blackler, R. J., Müller-Loennies, S., Brooks, C. L., Evans, D. W., Brade, L., Kosma, P., Brade, H., and Evans, S. V. (2011) A common NH53K mutation in the combining site of antibodies raised against chlamydial LPS glycoconjugates significantly increases avidity. *Biochemistry* **50,** 3357–3368
63. Brooks, C. L., Müller-Loennies, S., Brade, L., Kosma, P., Hirama, T., MacKenzie, C. R., Brade, H., and Evans, S. V. (2008) Exploration of specificity in germline monoclonal antibody recognition of a range of natural and synthetic epitopes. *J. Mol. Biol.* **377,** 450–468
64. Nguyen, H. P., Seto, N. O., MacKenzie, C. R., Brade, L., Kosma, P., Brade, H., and Evans, S. V. (2003) Germline antibody recognition of distinct carbohydrate epitopes. *Nat. Struct. Biol.* **10,** 1019–1025
65. Vranken, W., Tolkatchev, D., Xu, P., Tanha, J., Chen, Z., Narang, S., and Ni, F. (2002) Solution structure of a llama single-domain antibody with hydrophobic residues typical of the VH/VL interface. *Biochemistry* **41,** 8570–8579
66. Deng, S. J., MacKenzie, C. R., Sadowska, J., Michniewicz, J., Young, N. M., Bundle, D. R., and Narang, S. A. (1994) Selection of antibody single-chain variable fragments with improved carbohydrate-binding by phage display. *J. Biol. Chem.* **269,** 9533–9538
67. Kaminski, M. J., MacKenzie, C. R., Mooibroek, M. J., Dahms, T. E., Hirama, T., Houghton, A. N., Chapman, P. B., and Evans, S. V. (1999) The role of homophilic binding in anti-tumor antibody R24 recognition of molecular surfaces. Demonstration of an intermolecular beta-sheet interaction between vh domains. *J. Biol. Chem.* **274,** 5597–5604